CrossMark

# Cessation of Newtonian circular and plane Couette flows with wall slip and non-zero slip yield stress

**Maria Philippou · Yiolanda Damianou · Xenia Miscouridou · Georgios C. Georgiou**

**Abstract**  We solve analytically the cessation flows of a Newtonian fluid in circular and plane Couette geometries assuming that wall slip occurs provided that the wall shear stress exceeds a critical threshold, the slip yield stress. In steady-state, slip occurs only beyond a critical value of the angular velocity of the rotating inner cylinder in circular Couette flow or of the speed of the moving upper plate in plane Couette flow. Hence, in cessation, the classical no-slip solution holds if the corresponding wall speed is below the critical value. Otherwise, slip occurs only initially along both walls. Beyond a first critical time, slip along the fixed wall ceases, and beyond a second critical time slip ceases also along the initially moving wall. Beyond this second critical time no slip is observed and the decay of the velocity is faster. The velocity decays exponentially in all regimes and the decay is reduced with slip. The effects of slip and the slip yield stress are discussed.

**Keywords**  Circular Couette flow · Plane Couette flow · Newtonian Fluid · Slip · Slip yield stress · Cessation flow

M. Philippou · Y. Damianou · G. C. Georgiou (✉)
Department of Mathematics and Statistics, University of Cyprus, P.O. Box 20537, 1678 Nicosia, Cyprus
e-mail: georgios@ucy.ac.cy

X. Miscouridou
Department of Mathematics, Imperial College London, London SW7 2AZ, UK

## 1 Introduction

The role of wall slip is important in many applications, such as the extrusion of complex fluids, ink jet processes, oil migration in porous media, and in microfluidics. The occurrence of slip has been documented for many fluids both experimentally and theoretically [1, 2]. Experimental studies of wall slip with Newtonian liquids have been reviewed by Neto et al. [3] and Lauga et al. [4]. The occurrence of slip has also been observed in nanoscale experiments [5] and in molecular dynamic simulations [6].

The most common slip equation is Navier's slip law [7] which relates the wall shear stress, $\tau_w$, to the slip velocity, $u_w$, defined as the velocity of the fluid relative to that of the wall:

$$\tau_w = \beta u_w, \tag{1}$$

where $\beta$ is the slip coefficient, which is in general a function of temperature, normal stress and pressure, and the characteristics of the fluid/wall interface [8]. The no-slip boundary condition is recovered when $\beta \to \infty$. The slip coefficient is related to the so-called slip length $b$, i.e. $\beta \equiv \eta/b$, where $\eta$ denotes the viscosity [9]. Different methods have been proposed in order to account for wall slip and improve the rheological characterization of materials for correcting the rheological parameters from Couette rheometers (see [10] and references therein). Works concerned with analytical solutions of Newtonian flows with Navier slip have been reviewed by

Kaoullas and Georgiou [11, 12]. Ferrás et al. [13] presented analytical solutions of various Newtonian and inelastic non-Newtonian Couette and Poiseuille flows using a non-linear (power-law) slip equation in addition to Navier slip. Recently, Ng [14] also reported a collection of analytical solutions for starting Newtonian Couette and Poiseuille flows with Navier slip in many different geometries of interest (e.g. in plane, round, annular and rectangular tubes for the latter flow).

In many experimental studies on various fluid systems, it has been observed that wall slip occurs only above a certain critical value of the wall shear stress, known as the slip yield stress, $\tau_c$ [15–17]. Spikes and Granick [18] proposed the following two-branch extension of Navier's slip equation for Newtonian fluid flow:

$$\begin{cases} u_w = 0, & \tau_w \leq \tau_c \\ \tau_w = \tau_c + \beta u_w, & \tau_w > \tau_c \end{cases}. \qquad (2)$$

A number of other slip equations involving slip yield stress (also referred to as threshold slip equations) have been proposed based on experiments with different materials (see [16] and references therein). The two-branch form of Eq. (2) leads to some interesting theoretical as well as numerical difficulties, analogous to those encountered with the discontinuous Bingham-plastic constitutive model [16, 19]. Different flow regimes are defined by critical values for the occurrence of slip along a wall. For example, in Poiseuille and in simple shear flows, slip occurs only above a critical value of the imposed pressure gradient [11]. Moreover, in 2D and 3D, slip may occur only along unknown parts of the wall which is of interest both physically and numerically [20]. Recently, analytical solutions of steady-state and transient pressure-driven Newtonian flows in various geometries with wall slip governed by Eq. (2) have been derived [11, 12, 17, 21].

A recent work involving a slip equation with non-zero slip yield stress is that of Tauviqirrahman et al. [22] who analyzed the effects of surface texturing and wall slip on the load-carrying capacity of parallel sliding systems. Bryan et al. [23] studied both experimentally and numerically the extrusion flow of a viscoplastic material through axisymmetric square entry dies. They concluded that the linear Navier-slip model (1) is not adequate to describe the experimental

flows and that further numerical simulations with slip Eq. (2) are necessary.

The objective of the present work is to derive analytical solutions for the cessation of Newtonian circular and plane Couette flows with wall slip and non-zero slip yield stress. Both flows are standard viscometric flows and their analytical solutions are missing from the recent compilations of Ng [14] and Kaoullas and Georgiou [11, 12]. The circular Couette flow, i.e. the flow between coaxial cylinders one of which is rotating while the other is kept fixed, is widely used for the rheological characterization of complex fluids [24]. Possible sources of error in determining the rheological parameters include end effects, eccentricities, viscous heating, and wall slip [24]. The analytical solutions derived below may be useful in studies involving start up and cessation of steady shear in rheometric and microfluidic devices, in tribology, and in testing numerical codes implementing slip Eq. (2). The steady-state circular and plane Couette flows are analyzed in Sects. 2 and 3, respectively, where the general cases of walls of different properties are also considered and different flow regimes depending on the speed of the moving boundary are identified. In Sect. 4, the solution of the cessation of circular Couette flow is derived and discussed. The cessation of plane Couette flow is investigated in Sect. 5. Finally, the conclusions of this work are provided in Sect. 6.

## 2 Steady circular Couette flow

We consider the steady circular Couette flow of a Newtonian fluid. The radii of the inner and outer cylinders are $\kappa R$ and $R$, respectively, where $0 < \kappa < 1$, as illustrated in Fig. 1. The inner cylinder is rotating at an angular velocity $\Omega$ and the gravitational acceleration is zero. The two cylinders are assumed to be infinitely long and the flow is axisymmetric.

### 2.1 Navier slip

We first consider the general case in which Navier slip occurs along both the inner and outer cylinders and denote the two slip velocities by $u_{w1}$ and $u_{w2}$, respectively. We also allow the possibility of different slip coefficients along the two walls so that
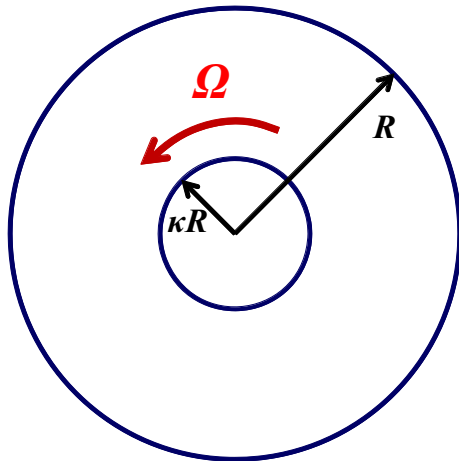
**Fig. 1** Geometry of circular Couette flow

$$\tau_{wi} = \beta_i u_{wi}, \quad i = 1, 2, \tag{3}$$

where $\tau_{w1}$ and $\tau_{w2}$ are the wall shear stresses along the two walls. The general form of the steady-state azimuthal velocity is [25]:

$$u_\theta(r) = c_1 r + \frac{c_2}{r}. \tag{4}$$

The constants $c_1$ and $c_2$ are determined by applying the boundary conditions

$$u_\theta(\kappa R) = \kappa \Omega R - u_{w1} \tag{5}$$

and

$$u_\theta(R) = u_{w2}, \tag{6}$$

which gives

$$u_\theta(r) = \frac{\kappa^2 \Omega R}{1 - \kappa^2 + 2B_1 + 2\kappa^3 B_2} \left[ \frac{R}{r} - (1 - 2\kappa B_2) \frac{r}{R} \right], \tag{7}$$

where $B_1$ and $B_2$ are the dimensionless slip numbers defined by

$$B_i \equiv \frac{\eta}{\beta_i \kappa R}, \quad i = 1, 2. \tag{8}$$

It should be noted that the slip coefficient appears in the denominator of the slip number. Hence, the no-slip boundary conditions is recovered by setting $B_i = 0$. For the shear stress $\tau_{r\theta} = \eta r d(u_\theta/r)/dr$ one finds that

$$\tau_{r\theta} = -\frac{2\eta \kappa^2 \Omega R^2}{1 - \kappa^2 + 2B_1 + 2\kappa^3 B_2} \frac{1}{r^2}. \tag{9}$$

Therefore, the two wall shear stresses are

$$\tau_{w1} = \frac{2\eta \Omega}{1 - \kappa^2 + 2B_1 + 2\kappa^3 B_2} \tag{10}$$

and

$$\tau_{w2} = \kappa^2 \tau_{w1}. \tag{11}$$

It should be noted that Eq. (11) holds irrespective of the wall boundary conditions. Finally, for the two slip velocities we find

$$u_{w1} = \frac{2\kappa B_1 \Omega R}{1 - \kappa^2 + 2B_1 + 2\kappa^3 B_2} \quad \text{and } u_{w2} = \frac{B_2}{B_1} \kappa^2 u_{w1}. \tag{12}$$

If the same slip law applies to both cylinders $(\beta_1 = \beta_2 = \beta)$, then the velocity is given by

$$u_\theta(r) = \frac{\kappa^2 \Omega R}{1 - \kappa^2 + 2(1 + \kappa^3)B} \left[ \frac{R}{r} - (1 - 2\kappa B) \frac{r}{R} \right], \tag{13}$$

where $B \equiv \eta/(\beta \kappa R)$. In this case, we have for the two slip velocities

$$u_{w1} = \frac{2\kappa B \Omega R}{1 - \kappa^2 + 2(1 + \kappa^3)B} = \frac{u_{w2}}{\kappa^2}, \tag{14}$$

while

$$\tau_{w1} = \frac{2\eta \Omega}{1 - \kappa^2 + 2(1 + \kappa^3)B}. \tag{15}$$

It is clear that setting $B_1 = 0$ (and/or $B_2 = 0$) the special solution when we have no slip along the inner (and/or the outer) wall is obtained. The various special cases of interest are illustrated in Fig. 2 along with the corresponding expressions of the velocity and the slip velocities.

Scaling the azimuthal velocity by $\kappa \Omega R$ and $r$ by $R$ and denoting dedimensionalized quantities by stars, we can write

$$u_\theta^*(r^*) = \frac{\kappa}{1 - \kappa^2 + 2(1 + \kappa^3)B} \left[ \frac{1}{r^*} - (1 - 2\kappa B)r^* \right]. \tag{16}$$

In Fig. 3a, we plotted $u_\theta^*$ for $\kappa = 0.5$ and various values of the slip number $B$. We observe that the velocity at the outer cylinder $u_\theta^*(1) = u_{w2}^*$ increases while $u_\theta^*(\kappa) = 1 - u_{w1}^*$ decreases with $B$. Eventually,
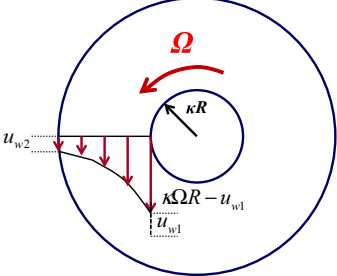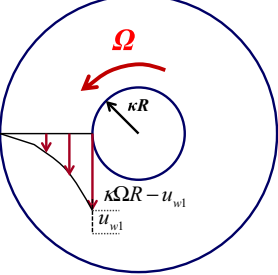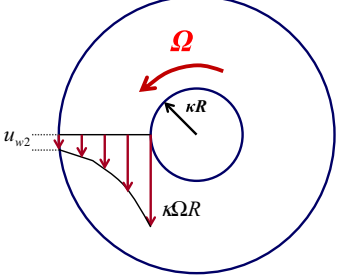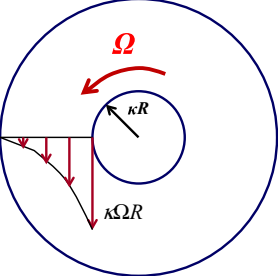
| **(a) Slip along both cylinders** | $u_\theta(r) = \dfrac{\kappa^2\Omega R}{1-\kappa^2+2(1+\kappa^3)B}\left[\dfrac{R}{r}-(1-2\kappa B)\dfrac{r}{R}\right]$ $\tau_{w1} = \dfrac{2\eta\,\Omega}{1-\kappa^2+2(1+\kappa^3)B}$ $u_{w1} = \dfrac{2\kappa B\,\Omega R}{1-\kappa^2+2(1+\kappa^3)B}$ $u_{w2} = \kappa^2 u_{w1}$ |
|---|---|
| **(b) Slip only along the inner cylinder** | $u_\theta(r) = \dfrac{\kappa^2\Omega R}{1-\kappa^2+2B}\left(\dfrac{R}{r}-\dfrac{r}{R}\right)$ $\tau_{w1} = \dfrac{2\eta\,\Omega}{1-\kappa^2+2B}$ $u_{w1} = \dfrac{2\kappa B\,\Omega R}{1-\kappa^2+2B}$ $u_{w2} = 0$ |
| **(c) Slip only along the outer cylinder** | $u_\theta(r) = \dfrac{\kappa^2\Omega R}{1-\kappa^2+2\kappa^3 B}\left[\dfrac{R}{r}-(1-2\kappa B)\dfrac{r}{R}\right]$ $\tau_{w1} = \dfrac{2\eta\,\Omega}{1-\kappa^2+2\kappa^3 B}$ $u_{w1} = 0$ $u_{w2} = \dfrac{2\kappa^3 B\,\Omega R}{1-\kappa^2+2\kappa^3 B}$ |
| **(d) No-slip along both cylinders** | $u_\theta(r) = \dfrac{\kappa^2\Omega R}{1-\kappa^2}\left(\dfrac{R}{r}-\dfrac{r}{R}\right)$ $\tau_{w1} = \dfrac{2\eta\,\Omega}{1-\kappa^2}$ $u_{w1} = u_{w2} = 0$ |

**Fig. 2** Different cases of Navier slip in circular Couette flow with the corresponding solutions
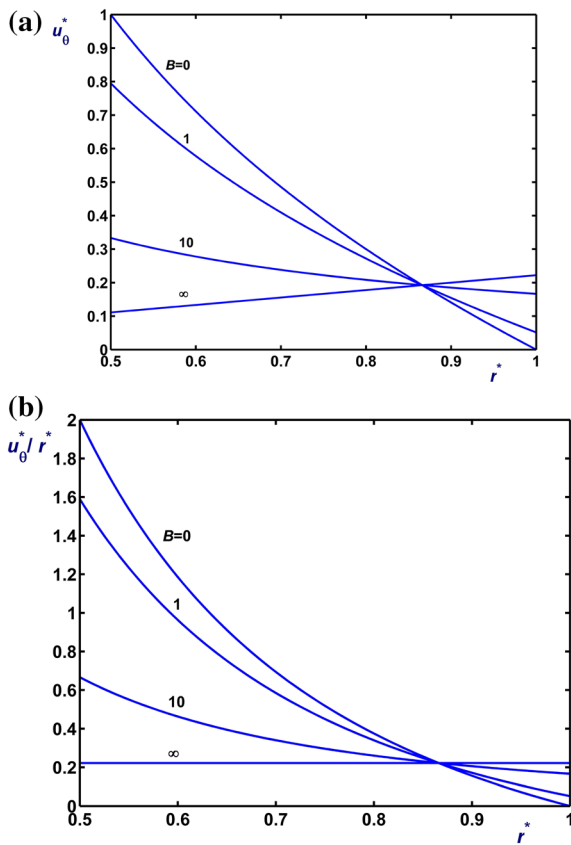
**Fig. 3** Velocity profiles in circular Couette flow with Navier slip for $\kappa = 0.5$ and various slip numbers: (a) azimuthal velocity; (b) angular velocity

$u_\theta^*$ becomes an increasing function of $r^*$ and in the limit of infinite $B$ (full slip) $u_\theta^*$ becomes linear:

$$u_\theta^*(r^*) \rightarrow \frac{\kappa^2}{1 + \kappa^3} r^*. \tag{17}$$

Moreover, all velocity profiles have a common point at $r^* = \sqrt{1 - \kappa + \kappa^2}$. The corresponding plot of the angular velocity $u_\theta^*/r^*$ is shown in Fig. 3b. As expected, the angular velocity is always a decreasing function of $r^*$ and becomes flat (solid body rotation) in the limit of full slip. The asymptotic value of the angular velocity is $\kappa^2/(1 + \kappa^3)$.

### 2.2 Slip with non-zero slip yield stress

For simplicity, we consider the case in which the same slip law with a slip coefficient $\beta$ and a slip yield stress $\tau_c$ applies along both cylinders. It is clear that below a critical angular velocity $\Omega_1$ no slip occurs and the

expressions of case D in Fig. 2 apply. From Eq. (11) it is deduced that $\tau_{w1} > \tau_{w2}$, which implies that if the angular velocity is increased just above $\Omega_1$ slip occurs only along the inner cylinder. The angular velocity $\Omega_1$ corresponds to $\tau_{w1} = \tau_c$, which gives

$$\Omega_1 = \frac{(1 - \kappa^2)\tau_c}{2\eta}. \tag{18}$$

If $\Omega_2$ is the critical angular velocity for the occurrence of slip along the outer cylinder, then when $\Omega_1 < \Omega \le \Omega_2$ slip occurs only along the inner cylinder and the azimuthal velocity is given by

$$u_\theta = \frac{\tau_c R \kappa^2 (\eta\Omega/\tau_c + B)}{\eta(1 - \kappa^2 + 2B)} \left( \frac{R}{r} - \frac{r}{R} \right). \tag{19}$$

The shear stress and the slip velocity at the inner wall are given by

$$\tau_{w1} = \frac{2\tau_c(\eta\Omega/\tau_c + B)}{1 - \kappa^2 + 2B} \tag{20}$$

and

$$u_{w1} = \frac{\tau_c R \kappa B(2\eta\Omega/\tau_c - 1 + \kappa^2)}{\eta(1 - \kappa^2 + 2B)}. \tag{21}$$

The critical angular velocity $\Omega_2$ corresponds to $\tau_{w2} = \tau_c$, from which one gets

$$\Omega_2 = \frac{(1 - \kappa^2)(1 + 2B)\tau_c}{2\kappa^2\eta}. \tag{22}$$

In the last regime, $\Omega > \Omega_2$, slip occurs along both cylinders and the azimuthal velocity is given by

$$u_\theta = \frac{\tau_c R}{\eta} \left\{ \frac{\kappa^2[\eta\Omega/\tau_c + (1 + \kappa)B]}{1 - \kappa^2 + 2(1 + \kappa^3)B} \left[ \frac{R}{r} - (1 - 2\kappa B)\frac{r}{R} \right] \right. $$
$$\left. - \kappa B \frac{r}{R} \right\}. \tag{23}$$

For the wall shear stress along the inner cylinder we get

$$\tau_{w1} = \frac{2[\eta\Omega/\tau_c + (1 + \kappa)B]\tau_c}{1 - \kappa^2 + 2(1 + \kappa^3)B}, \tag{24}$$

while the two slip velocities are given by

$$u_{w1} = \frac{\tau_c R \kappa B[2\eta\Omega/\tau_c - (1 - \kappa^2)(1 - 2\kappa B)]}{\eta[1 - \kappa^2 + 2(1 + \kappa^3)B]} \tag{25}$$

and

$$u_{w2} = \frac{\tau_c R \kappa B [2\eta \kappa^2 \Omega/\tau_c - (1-\kappa^2)(1-2\kappa B)]}{\eta[1-\kappa^2 + 2(1+\kappa^3)B]}. \tag{26}$$

In this case, it is more convenient to dedimensionalize the solution by scaling the azimuthal velocity $u_\theta$ by $\tau_c R/\eta$, the angular velocity by $\tau_c/\eta$, and the shear stress by $\tau_c$. Thus, the two dimensionless critical angular velocities are

$$\Omega_1^* = \frac{1-\kappa^2}{2} \tag{27}$$

and

$$\Omega_2^* = \frac{(1-\kappa^2)(1+2B)}{2\kappa^2}. \tag{28}$$

The azimuthal velocity and the inner-cylinder shear stress are given by

$$u_\theta^* = \begin{cases} \dfrac{\kappa^2 \Omega^*}{1-\kappa^2}\left(\dfrac{1}{r^*} - r^*\right), & \Omega^* \le \Omega_1^* \\[2mm] \dfrac{\kappa^2(\Omega^* + B)}{1-\kappa^2 + 2B}\left(\dfrac{1}{r^*} - r^*\right), & \Omega_1^* < \Omega^* \le \Omega_2^* \\[2mm] \dfrac{\kappa^2[\Omega^* + (1+\kappa)B]}{1-\kappa^2 + 2(1+\kappa^3)B}\left[\dfrac{1}{r^*} - (1-2\kappa B)r^*\right] - \kappa B r^*, & \Omega^* > \Omega_2^* \end{cases} \tag{29}$$

and

$$\tau_{w1}^* = \begin{cases} \dfrac{2\Omega^*}{1-\kappa^2}, & \Omega^* \le \Omega_1^* \\[2mm] \dfrac{2(\Omega^* + B)}{1-\kappa^2 + 2B}, & \Omega_1^* < \Omega^* \le \Omega_2^* \\[2mm] \dfrac{2[\Omega^* + (1+\kappa)B]}{1-\kappa^2 + 2(1+\kappa^3)B}, & \Omega^* > \Omega_2^* \end{cases}. \tag{30}$$

Finally, for the two slip velocities we get:

$$u_{w1} = \kappa B \begin{cases} 0, & \Omega^* \le \Omega_1^* \\[2mm] \dfrac{2\Omega^* - (1-\kappa^2)}{1-\kappa^2 + 2B}, & \Omega_1^* < \Omega^* \le \Omega_2^* \\[2mm] \dfrac{2\Omega^* - (1-\kappa^2)(1-2\kappa B)}{1-\kappa^2 + 2(1+\kappa^3)B}, & \Omega^* > \Omega_2^* \end{cases} \tag{31}$$

and

$$u_{w2}^* = \kappa B \begin{cases} 0, & \Omega^* \le \Omega_2^* \\[2mm] \dfrac{2\kappa^2 \Omega^* - (1-\kappa^2)(1+2B)}{1-\kappa^2 + 2(1+\kappa^3)B}, & \Omega^* > \Omega_2^* \end{cases}. \tag{32}$$

It is easily verified that the azimuthal velocity profiles when $\Omega^* = \Omega_1^*$ and $\Omega_2^*$ are respectively

$$u_\theta^* = \frac{\kappa^2}{2}\left(\frac{1}{r^*} - r^*\right) \quad \text{and} \quad u_\theta^* = \frac{1}{2}\left(\frac{1}{r^*} - r^*\right). \tag{33}$$

These profiles are independent of the slip number $B$ but it should be noted that $\Omega_2^*$ varies linearly with it. In Fig. 4, the angular velocities $u_\theta^*/r^*$ for $\kappa = 0.5$ corresponding to $\Omega_1^*, \Omega_2^*$, and to $2\Omega_2^*$ with various slip numbers are plotted. For small values of $B$ (weak slip), the effect of $B$ is more pronounced near the outer wall (where the shear stress is lower).
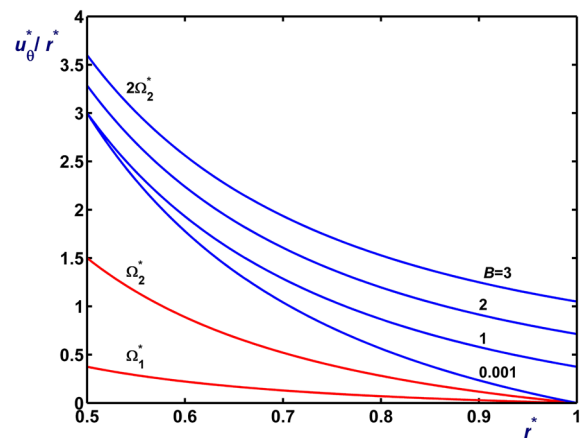


**Fig. 4** Azimuthal velocity profiles in circular Couette flow with $\kappa = 0.5$ in the case of non-zero slip yield stress. The profiles for $\Omega^* = \Omega_1^*$ and $\Omega_2^*$ are independent of the slip number $B$
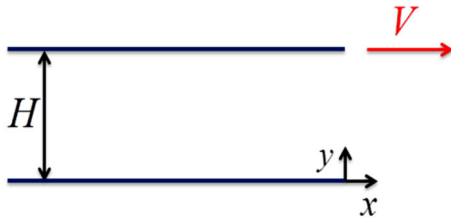
**Fig. 5** Geometry of plane Couette flow

## 3 Steady plane Couette flow

\We consider the steady flow of a Newtonian fluid between two infinite parallel plates, placed at a distance $H$ apart, assuming that the upper plate is moving with a speed $V$ while the lower one is fixed, as shown in Fig. 5.

### 3.1 Navier slip

In the general case Navier slip occurs along both walls but with different slip coefficients so that $\tau_{wi} = \beta_i u_{wi}$, $i = 1, 2$, where $\tau_{w1}$ and $\tau_{w2}$ are the wall shear stresses along the lower and upper walls, respectively. The general form of the steady-state velocity is simply $u_x(y) = c_1 y + c_2$. The constants $c_1$ and $c_2$ are determined by applying the boundary conditions $u_x(0) = u_{w1}$ and $u_x(H) = V - u_{w2}$. Thus, the fluid velocity is given by

$$u_x(y) = \frac{V}{1 + B_1 + B_2}\left(\frac{y}{H} + B_1\right), \tag{34}$$

where $B_i \equiv \eta/\beta_i H$, $i = 1, 2$. The shear stress $\tau_{xy} = \eta du_x/dy$ is constant and therefore:

$$\tau_{w1} = \tau_{w2} = \frac{\eta}{1 + B_1 + B_2}\frac{V}{H}. \tag{35}$$

For the two slip velocities one finds

$$u_{w1} = \frac{B_1}{1 + B_1 + B_2}V$$
$$\text{and } u_{w2} = \frac{B_2}{1 + B_1 + B_2}V = \frac{B_2}{B_1}u_{w1}. \tag{36}$$

The various special cases of interest are illustrated in Fig. 6 along with the corresponding expressions of the velocity and the slip velocities.

### 3.2 Slip with non-zero slip yield stress

As in Sect. 2, we consider only the case in which the same slip law with non-zero slip yield stress applies

along both walls. Below a critical velocity $V_c$ of the upper plate no slip occurs (case D in Fig. 6). Setting $\tau_w = \tau_c$ we get from Eq. (35)

$$V_c = \frac{H\tau_c}{\eta}. \tag{37}$$

The velocity is given by

$$u_x = \begin{cases} \dfrac{y}{H}V, & V \leq V_c \\ \dfrac{V_c}{1 + 2B}\left[(V/V_c + 2B)\dfrac{y}{H} + B(V/V_c - 1)\right], & V > V_c \end{cases}. \tag{38}$$

The shear stress is constant, and thus the wall shear stress along both plates is

$$\tau_w = \begin{cases} \dfrac{\eta V}{H}, & V \leq V_c \\ \tau_c + \dfrac{\dfrac{\tau_c}{V_c}(V - V_c)}{1 + 2B}, & V > V_c \end{cases}. \tag{39}$$

Obviously, the slip velocities along the two plates are the same:

$$u_w = \begin{cases} 0, & V \leq V_c \\ \dfrac{B(V - V_c)}{1 + 2B}, & V > V_c \end{cases}. \tag{40}$$

## 4 Cessation of circular Couette flow

We consider the cessation of the circular Couette flow of a Newtonian fluid. The steady-state solution serves as the initial condition and at $t = 0$ the inner cylinder stops rotating. The equation governing the azimuthal velocity $u_\theta(r, t)$ is

$$\frac{\partial u_\theta}{\partial t} = v\left(\frac{\partial^2 u_\theta}{\partial r^2} + \frac{1}{r}\frac{\partial u_\theta}{\partial r} - \frac{1}{r^2}u_\theta\right), \tag{41}$$

where $v \equiv \eta/\rho$ is the kinematic viscosity.

### 4.1 Navier slip

In the general case in which Navier slip occurs along both cylinders with different slip coefficients, the boundary and initial conditions read:
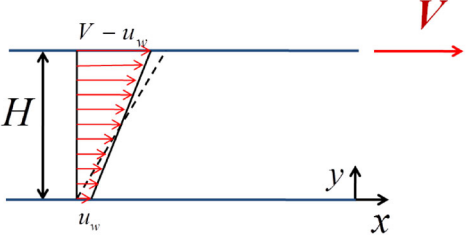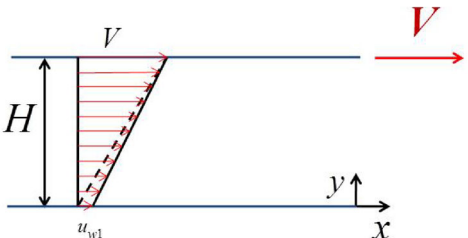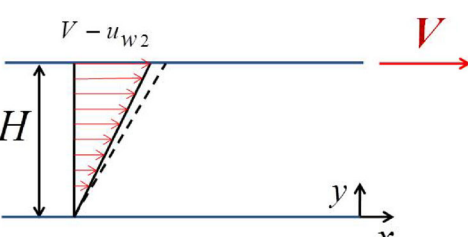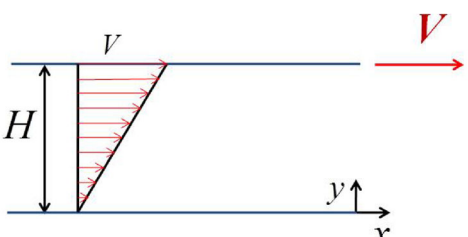
**(a)  Slip along both walls**

$$u_x(y) = \frac{V}{1+2B}\left(\frac{y}{H}+B\right)$$

$$\tau_w = \frac{\eta}{1+2B}\frac{V}{H}$$

$$u_{w1} = u_{w2} = \frac{B}{1+2B}V$$

**(b)  Slip only along the lower wall**

$$u_x(y) = \frac{V}{1+B_1}\left(\frac{y}{H}+B\right)$$

$$\tau_w = \frac{\eta}{1+B}\frac{V}{H}$$

$$u_{w1} = \frac{B}{1+B}V$$

$$u_{w2} = 0$$

**(c)  Slip only along the upper wall**

$$u_x(y) = \frac{V}{1+B}\frac{y}{H}$$

$$\tau_w = \frac{\eta}{1+B}\frac{V}{H}$$

$$u_{w1} = 0$$

$$u_{w2} = \frac{B}{1+B}V$$

**(d)  No-slip along both walls**

$$u_x(y) = V\frac{y}{H}$$

$$\tau_w = \eta\frac{V}{H}$$

$$u_{w1} = u_{w2} = 0$$

**Fig. 6**  Different cases of Navier slip in steady plane Couette flow

$$\left.\begin{array}{ll}
u_\theta(\kappa R, t) = \kappa B_1 R r \dfrac{\partial}{\partial r}\left(\dfrac{u_\theta}{r}\right)\bigg|_{r=\kappa R}, & t > 0 \\[12pt]
u_\theta(R, t) = -\kappa B_2 R r \dfrac{\partial}{\partial r}\left(\dfrac{u_\theta}{r}\right)\bigg|_{r=R}, & t \geq 0 \\[12pt]
u_\theta(r, 0) = \dfrac{\kappa^2 \Omega R}{1 - \kappa^2 + 2B_1 + 2\kappa^3 B_2}\left[\dfrac{R}{r} - (1 - 2\kappa B_2)\dfrac{r}{R}\right], & \kappa R \leq r \leq R
\end{array}\right\}. \tag{42}$$

The solution of the problem (41) and (42) is

$$u_\theta(r, t) = \sum_{k=1}^{\infty} C_k Z_{1k}\left(\frac{\lambda_k r}{R}\right) e^{\frac{-\lambda_k^2 \nu}{R^2} t}, \tag{43}$$

where $(\lambda_k, \gamma_k)$, $k = 1, 2, \ldots$ are the solutions of the system

$$\left.\begin{array}{l}
\kappa B_1 \lambda_k Z_{0k}(\kappa \lambda_k) - (1 + 2B_1)Z_{1k}(\kappa \lambda_k) = 0 \\
\kappa B_2 \lambda_k Z_{0k}(\lambda_k) + (1 - 2\kappa B_2)Z_{1k}(\lambda_k) = 0
\end{array}\right\}. \tag{44}$$

The functions $Z_{0k}$ and $Z_{1k}$ are defined by

$$\begin{array}{l}
Z_{0k}(r) \equiv J_0(r) + \gamma_k Y_0(r), \\
Z_{1k}(r) \equiv J_1(r) + \gamma_k Y_1(r),
\end{array} \tag{45}$$

where $J_1$, $J_2$ and $Y_0$, $Y_1$ are Bessel functions of the first and second kind, respectively. The constant $C_k$ is generally given by

$B_1 = B_2 = 0.5$ (same slip coefficient along the two cylinders). One may observe that cessation becomes slower (the eigenvalues $\lambda_k$ become smaller) in the presence of slip.

### 4.2 Slip with non-zero slip yield stress

As in Sect. 2.2, we consider the case in which the same slip law applies along both cylinders ($B_1 = B_2 = B$). We have seen that there are three flow regimes defined by the critical angular velocities $\Omega_1$ and $\Omega_2$. We will work with the dimensionless equations hereafter, obtained with the scales used in Sect. 2.2. In addition, time is now scaled by $\eta/\tau_c$.

*4.2.1 No slip ($\Omega^* \leq \Omega_1^*$)*

$$C_k = \frac{2\kappa^2(1 + 2B_1)(1 - 2\kappa B_2)^2 Z_{0k}(\kappa \lambda_k)\Omega R}{\lambda_k\left[(1 + 2B_1)^2(1 - 2\kappa B_2 + \kappa^2 B_2^2 \lambda_k^2)Z_{0k}^2(\lambda_k) - \kappa^2(1 - 2\kappa B_2)^2(1 + 2B_1 + \kappa^2 B_1^2 \lambda_k^2)Z_{0k}^2(\kappa \lambda_k)\right]}. \tag{46}$$

In the special case that $1 - 2\kappa B_2 = 0$, $C_k$ is simplified as follows:

$$C_k = \frac{2\kappa^2(1 + 2B_1)Z_{0k}(\kappa \lambda_k)\Omega R}{\lambda_k\left[(1 + 2B_1)^2 Z_{1k}^2(\lambda_k) - \kappa^2(1 + 2B_1 + \kappa^2 B_1^2 \lambda_k^2)Z_{0k}^2(\kappa \lambda_k)\right]}. \tag{47}$$

Various special cases can easily be obtained. Figure 7 illustrates three possibilities for the evolution of the dimensionless velocity (scaled by $\kappa \Omega R$) where time is scaled by $R^2/\nu$: (a) the classical no-slip solution obtained by setting $B_1 = B_2 = 0$; (b) the solution when slip occurs only along the inner wall ($B_2 = 0$) with $B_1 = 0.5$; and (c) the solution when

The no-slip solution can be found in many textbooks [25]:

$$u_\theta^*(r^*, t^*) = \sum_{k=1}^{\infty} C_k Z_{1k}(\lambda_k r^*) e^{-\lambda_k^2 t^*}, \tag{48}$$

where $(\lambda_k, \gamma_k)$, $k = 1, 2, \ldots$ are the solutions of the system

$$Z_{1k}(\kappa \lambda_k) = Z_{1k}(\lambda_k) = 0 \tag{49}$$

and $C_k$ is given by

$$C_k = \frac{2\kappa^2 \Omega^* Z_{0k}(\kappa \lambda_k)}{\lambda_k\left[Z_{0k}^2(\lambda_k) - \kappa^2 Z_{0k}^2(\kappa \lambda_k)\right]}. \tag{50}$$
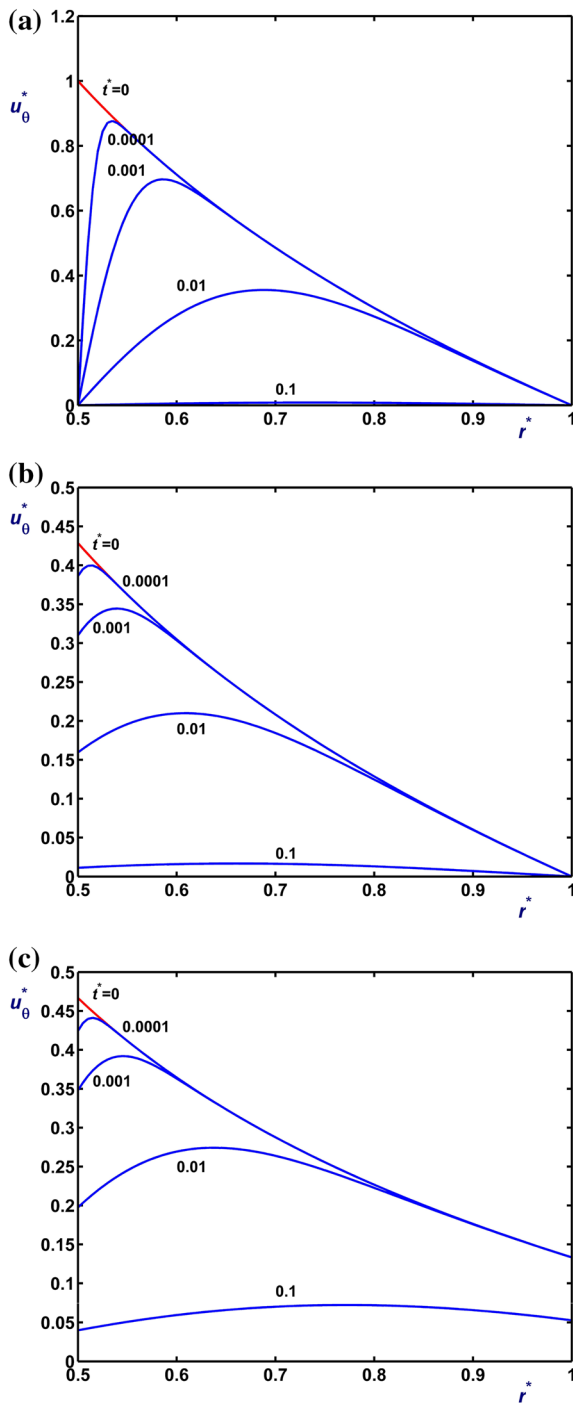
**Fig. 7** Cessation of circular Couette flow with $\kappa = 0.5$: (a) No-slip along both cylinders ($B_1 = B_2 = 0$); (b) Navier slip only along the inner cylinder ($B_1 = 0.5$, $B_2 = 0$); (c) Navier slip along both cylinders ($B_1 = B_2 = 0.5$)

### 4.2.2 Slip only along the inner cylinder ($\Omega_1^* < \Omega^* \leq \Omega_2^*$)

In this case the boundary and initial conditions read

$$
\left.
\begin{aligned}
u_\theta^*(\kappa, t^*) &= \kappa B\left[ r^* \frac{\partial}{\partial r^*}\left(\frac{u_\theta^*}{r^*}\right)\Big|_{r^*=\kappa} - 1 \right], & t^* > 0 \\
u_\theta^*(1, t^*) &= 0, & t^* \geq 0 \\
u_\theta^*(r^*, 0) &= \frac{\kappa^2(\Omega^* + B)}{1 - \kappa^2 + 2B}\left(\frac{1}{r^*} - r^*\right), & \kappa \leq r^* \leq 1
\end{aligned}
\right\}.
$$
(51)

The solution is then given by

$$
u_\theta^*(r^*, t^*)
$$
$$
= \begin{cases}
\sum_{n=1}^\infty A_n Z_{1n}(\alpha_n r^*)e^{-\alpha_n^2 t^*} - \dfrac{\kappa^2 B}{1-\kappa^2+2B}\left(\dfrac{1}{r^*} - r^*\right), & t^* \leq t_{c1}^* \\
\sum_{k=1}^\infty C_k Z_{1k}(\lambda_k r^*)e^{-\lambda_k^2(t^* - t_{c1}^*)}, & t^* > t_{c1}^*
\end{cases},
$$
(52)

where $(\alpha_n, \delta_n)$, $n = 1, 2, \ldots$ are the solutions of the system

$$
\left.
\begin{aligned}
\kappa B \alpha_n Z_{0n}(\kappa \alpha_n) - (1 + 2B)Z_{1n}(\kappa \alpha_n) &= 0 \\
Z_{1n}(\alpha_n) &= 0
\end{aligned}
\right\}
$$
(53)

with

$$
\begin{aligned}
Z_{0n}(r) &\equiv J_0(r) + \delta_n Y_0(r), \\
Z_{1n}(r) &\equiv J_1(r) + \delta_n Y_1(r)
\end{aligned}
$$
(54)

and $A_n$ and $C_k$ are respectively given by

$$
A_n = \frac{2\kappa^2(1+2B)(\Omega^*+2B)Z_{0n}(\kappa\alpha_n)}{\alpha_n\left[Z_{0n}^2(\alpha_n)(1+2B)^2 - \kappa^2 Z_{0n}^2(\kappa\alpha_n)(1+2B+\alpha_n^2\kappa^2 B^2)\right]}
$$
(55)

and

$$
\begin{aligned}
C_k =& \frac{2Z_{0k}(\kappa\lambda_k)}{\lambda_k\left[Z_{0k}^2(\lambda_k) - \kappa^2 Z_{0k}^2(\kappa\lambda_k)\right]} \\
&\times \left[\sum_{n=1}^\infty A_n \frac{\kappa\lambda_k^2}{\lambda_k^2 - \alpha_n^2}Z_{1n}(\kappa\alpha_n)e^{-\alpha_n^2 t_{c1}^*} - \frac{\kappa^2 B(1-\kappa^2)}{1-\kappa^2+2B}\right].
\end{aligned}
$$
(56)

The critical time $t_{c1}^*$, at which slip ceases along the inner wall is the root of the following equation:

$$
\sum_{n=1}^\infty A_n^* Z_{1n}(\alpha_n\kappa)e^{-\alpha_n^2 t^*} = \frac{\kappa B(1-\kappa^2)}{1-\kappa^2+2B}.
$$
(57)

The slip velocity at the inner cylinder is

$$u_{w1}^*(t^*)$$
$$= \begin{cases} \sum_{n=1}^{\infty} A_n Z_{1n}(\alpha_n \kappa) e^{-\alpha_n^2 t^*} - \dfrac{\kappa(1-\kappa^2)B}{1-\kappa^2+2B}, & t^* \leq t_{c1}^* \\ 0, & t^* > t_{c1}^* \end{cases}.$$

(58)

### 4.2.3 Slip along both cylinders ($\Omega^* > \Omega_2^*$)

In this case the boundary and initial conditions read

$$\left. \begin{array}{ll} u_\theta^*(\kappa, t^*) = \kappa B \left[ r^* \dfrac{\partial}{\partial r^*} \left( \dfrac{u_\theta^*}{r^*} \right) \Big|_{r^*=\kappa} - 1 \right], & t^* > 0 \\[3mm] u_\theta^*(1, t^*) = -\kappa B \left[ r^* \dfrac{\partial}{\partial r^*} \left( \dfrac{u_\theta^*}{r^*} \right) \Big|_{r^*=1} + 1 \right], & t^* \geq 0 \\[3mm] u_\theta^*(r^*, 0) = \dfrac{\kappa^2[\Omega^* + (1+\kappa)B]}{1-\kappa^2+2(1+\kappa^3)B} \left[ \dfrac{1}{r^*} - (1-2\kappa B)r^* \right] - \kappa B r^*, & \kappa \leq r^* \leq 1 \end{array} \right\}$$

(59)

and the solution is

$$u_\theta^*(r^*, t^*) = \begin{cases} \sum_{m=1}^{\infty} A_m Z_{1m}(\mu_m r^*) e^{-\mu_m^2 t^*} - \dfrac{(1-\kappa)\kappa^2 B}{1-\kappa^2+2(1+\kappa^3)B} \left[ \dfrac{1}{r^*} - (1-2\kappa B)r^* \right] - \kappa B r^*, & t^* \leq t_{c1}^* \\[4mm] \sum_{n=1}^{\infty} C_n Z_{1n}(\alpha_n r^*) e^{-\alpha_n^2 (t^* - t_{c1}^*)} - \dfrac{\kappa^2 B}{1-\kappa^2+2B} \left( \dfrac{1}{r^*} - r^* \right), & t_{c1}^* < t^* \leq t_{c2}^* \\[4mm] \sum_{k=1}^{\infty} D_k Z_{1k}(\lambda_k r^*) e^{-\lambda_k^2 (t^* - t_{c2}^*)}, & t^* > t_{c2}^* \end{cases}.$$

(60)

Here $(\mu_m, \varepsilon_m)$, $k = 1, 2, \ldots$ are the solutions of the system

$$\left. \begin{array}{l} \kappa B \mu_m Z_{0m}(\kappa\mu_m) - (1+2B)Z_{1m}(\kappa\mu_m) = 0 \\ \kappa B \mu_m Z_{0m}(\mu_m) + (1-2\kappa B)Z_{1m}(\mu_m) = 0 \end{array} \right\},$$

(61)

where

$$\begin{array}{l} Z_{0m}(r) \equiv J_0(r) + \varepsilon_m Y_0(r), \\ Z_{1m}(r) \equiv J_1(r) + \varepsilon_m Y_1(r) \end{array}$$

(62)

and $A_m$, $C_n$ and $D_k$ are given by

$$A_m = \frac{2\kappa^2(\Omega^* + 2B)Z_{0m}(\kappa\mu_m)}{\mu_m(1+2B)\left[ Z_{0m}^2(\mu_m) \frac{(1-2\kappa B+\kappa^2\mu_m^2 B^2)}{(1-2\kappa B)^2} - \kappa^2 Z_{0m}^2(\kappa\mu_m) \frac{(1+2B+\kappa^2\mu_m^2 B^2)}{(1+2B)^2} \right]},$$
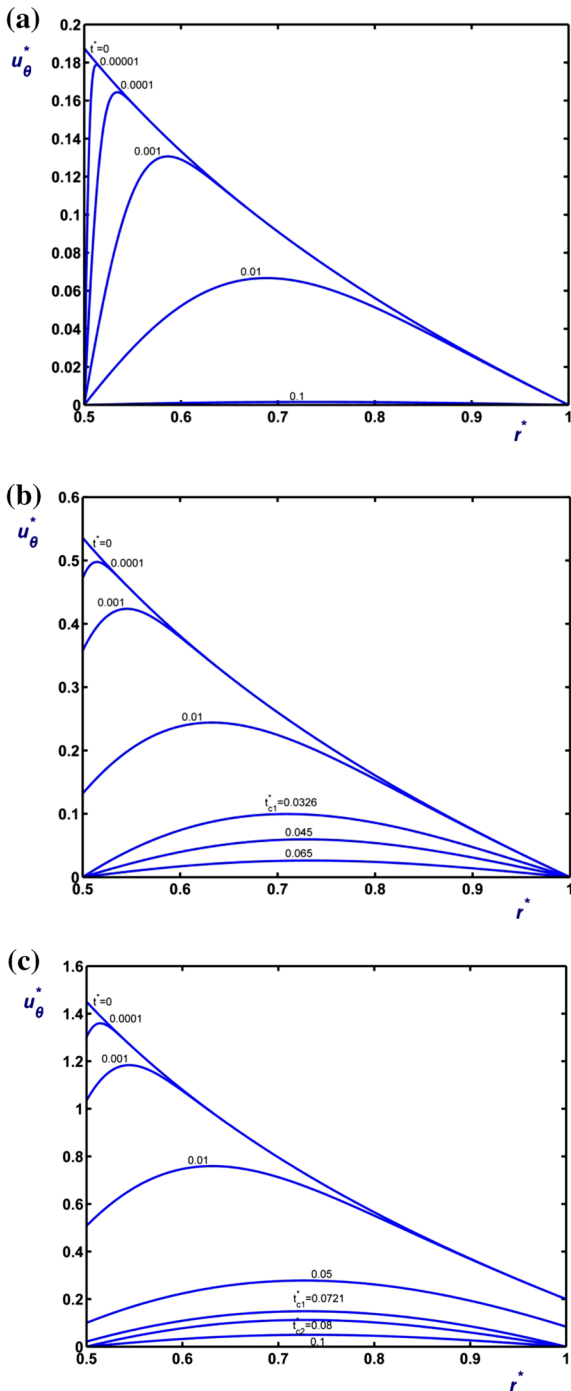
(63)

and

**(a)**



**(b)**



**(c)**



**Fig. 8** Cessation of circular Couette flow with $\kappa = 0.5$ and $B = 0.5$ and different initial conditions: (a) $\Omega^* = \Omega_1^* = 0.375$ (no slip initially); (b) $\Omega^* = \Omega_2^* = 3$ (slip only at the inner cylinder); and (c) $\Omega^* = 6 > \Omega_2^*$ (slip at both cylinders)
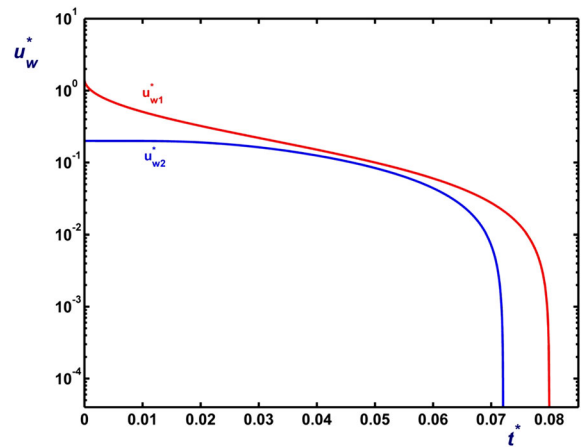


**Fig. 9** Evolution of the slip velocities in cessation of circular Couette flow for $\kappa = 0.5$, $B = 0.5$, and $\Omega^* = 6 > \Omega_2^*$
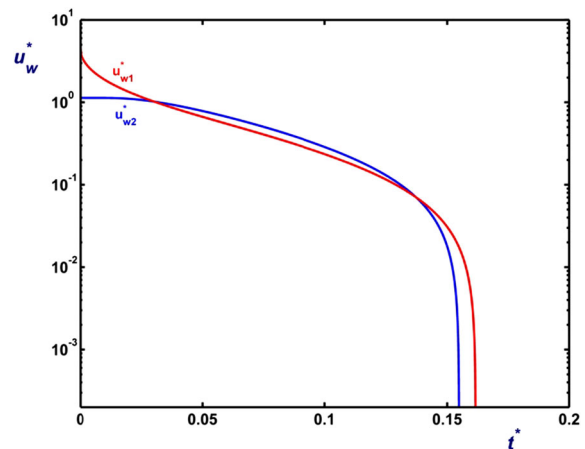


**Fig. 10** Evolution of the slip velocities in cessation of circular Couette flow for $\kappa = 0.5$, $B = 0.5$, and $\Omega^* = 20 > \Omega_2^*$

$$C_n = \frac{2(1 + 2B)^2 Z_{0n}(\alpha_n)}{\alpha_n \left[ Z_{0n}^2(\alpha_n)(1 + 2B)^2 - \kappa^2 Z_{0n}^2(\kappa\alpha_n)\left(1 + 2B + \alpha_n^2\kappa^2 B^2\right) \right]}$$

$$\times \left\{ \sum_{m=1}^{\infty} A_m e^{-\mu_m^{*2} t_{c1}^*} \left[ \frac{-\alpha_n^2 Z_{1m}(\mu_m)}{\alpha_n^2 - \mu_m^2} \right] + \frac{\kappa B[1 - \kappa^2 + 2(1 + \kappa^2)B]}{1 - \kappa^2 + 2(1 + \kappa^3)B} \right\} \tag{64}$$

$$D_k = \frac{2Z_{0k}(\kappa\lambda_k)}{\lambda_k \left[ Z_{0k}^2(\lambda_k) - \kappa^2 Z_{0k}^2(\kappa\lambda_k) \right]}$$

$$\times \left[ \sum_{n=1}^{\infty} C_n e^{-a_k^2 \left( t_{c2}^* - t_{c1}^* \right)} \frac{\kappa\lambda_k^2}{\lambda_k^2 - \alpha_n^2} Z_{1n}(\kappa\alpha_n) - \frac{\kappa^2(1 - \kappa^2)B}{1 - \kappa^2 + 2B} \right]. \tag{65}$$

The critical time $t_{c1}^*$, at which slip no longer occurs along the outer cylinder, and the critical time $t_{c2}^*$, at which slip ceases along the inner cylinder are respectively the roots of

$$\sum_{m=1}^{\infty} A_m Z_{1m}(\mu_m) e^{-\mu_m^2 t^*} = \frac{\kappa B_2[1 - \kappa^2 + 2(1 + \kappa^2)B]}{1 - \kappa^2 + 2(1 + \kappa^3)B} \tag{66}$$

and

$$\sum_{n=1}^{\infty} C_n Z_{1n}(\kappa\alpha_n) e^{-\alpha_n^2 \left( t^* - t_{c1}^* \right)} = \frac{\kappa(1 - \kappa^2)B}{1 - \kappa^2 + 2B}. \tag{67}$$

Finally, the two slip velocities are given by

$$u_{w1}^*(t^*)$$
$$= \begin{cases} \sum_{m=1}^{\infty} A_m Z_{1m}(\mu_m) e^{-\mu_m^2 t^*} - \frac{\kappa B[1 - \kappa^2 + 2(1 + \kappa^2)B]}{1 - \kappa^2 + 2(1 + \kappa^3)B}, & t^* \leq t_{c1}^* \\ 0, & t^* > t_{c1}^* \end{cases} \tag{68}$$

and

$$u_{w2}^*(t^*) = \begin{cases} \sum_{m=1}^{\infty} A_m Z_{1m}(\kappa\mu_m) e^{-\mu_m^2 t^*} - \frac{\kappa(1 - \kappa)B}{1 - \kappa^2 + 2(1 + \kappa^3)B} \left[ 1 - (1 - 2\kappa B)\kappa^2 \right] - \kappa^2 B, & t^* \leq t_{c1}^* \\ \sum_{n=1}^{\infty} C_n Z_{1n}(\kappa\alpha_n) e^{-\alpha_n^2 \left( t^* - t_{c1}^* \right)} - \frac{\kappa(1 - \kappa^2)B}{1 - \kappa^2 + 2B}, & t_{c1}^* < t^* \leq t_{c2}^* \\ 0, & t^* > t_{c2}^* \end{cases} \tag{69}$$

The evolution of the velocity for $\kappa = 0.5$ and $B = 0.5$ is illustrated in Fig. 8 for three representative values of the angular velocity: (a) $\Omega^* = \Omega_1^* = 0.375$ such that

no slip occurs from $t^* = 0$ and the classical cessation solution holds; (b) $\Omega^* = \Omega_2^* = 3$ such that slip occurs only at the inner cylinder and ceases at $t_{c1}^* = 0.0426$; and (c) $\Omega^* = 6 > \Omega_2^*$ such that initially slip occurs everywhere and ceases along the outer cylinder at $t_{c1}^* = 0.0721$ and along the inner cylinder at $t_{c2}^* = 0.08$. The evolution of the two slip velocities in the latter case is shown in Fig. 9. Initially the slip velocity $u_{w2}^*$ along the outer cylinder appears to be rather constant but later it decays fast and vanishes earlier than $u_{w1}^*$. Our calculations showed that $u_{w2}^*$ is not necessarily lower than $u_{w1}^*$ at all times. One such example is the flow for $\kappa = 0.5$ and $\Omega^* = 20$. As shown in Fig. 10, the slip velocity $u_{w1}^*$ at the inner cylinder initially decreases faster and becomes lower than $u_{w2}^*$ for a while, but then $u_{w2}^*$ starts decreasing rapidly and vanishes earlier than $u_{w1}^*$.

## 5 Cessation of plane Couette flow

In cessation of plane Couette flow, the upper plate stops moving at $t = 0$ and the steady-state solution serves as the initial condition. The governing equation is

$$\frac{\partial u_x}{\partial t} = v \frac{\partial^2 u_x}{\partial y^2}. \tag{70}$$

## 5.1 Navier slip

In the general case in which Navier slip occurs along both walls with different slip coefficients, the boundary and initial conditions read:

$$\left.\begin{aligned}
u_x(0,t) &= B_1 H \frac{\partial u_x}{\partial y}\Big|_{y=0}, & t &> 0 \\
u_x(H,t) &= -B_2 H \frac{\partial u_x}{\partial y}\Big|_{y=H}, & t &\geq 0 \\
u_x(y,0) &= \frac{V}{1+B_1+B_2}\left(\frac{y}{H}+B_1\right), & 0 &\leq y \leq H
\end{aligned}\right\}$$
(71)

The velocity is given by

$$u_x(y,t) = \sum_{k=1}^{\infty} C_k\left[\sin\left(\frac{\lambda_k y}{H}\right) + B_1\lambda_k\cos\left(\frac{\lambda_k y}{H}\right)\right]e^{-\nu\frac{\lambda_k^2}{H^2}t},$$
(72)

where $\lambda_k$ are the roots of

$$\tan(\lambda_k) = \frac{(B_1+B_2)\lambda_k}{B_1 B_2 \lambda_k^2 - 1}$$
(73)

and the constants $C_k$ are given by

$$C_k = \frac{2V\left(B_1^2\lambda_k^2+1\right)\left(B_2^2\lambda_k^2+1\right)\cos\lambda_k}{\lambda_k\left(B_1 B_2\lambda_k^2-1\right)\left[\left(B_1^2\lambda_k^2+B_1+1\right)\left(B_2^2\lambda_k^2+1\right)+B_2\left(B_1^2\lambda_k^2+1\right)\right]}.$$
(74)

The evolution of the velocity in various representative cases is illustrated in Fig. 11, where the velocity is scaled by $V$, lengths by $H$, and time by $H^2/\nu$, and non-dimensionalized variables are denoted by stars: (a) The classical no-slip solution obtained by setting $B_1 = B_2 = 0$; (b) the solution when slip occurs only along lower wall with $B_1 = 0.5$ and $B_2 = 0$; (c) the solution when slip occurs only along upper wall with $B_1 = 0$ and $B_2 = 0.5$; (d) the solution when $B_1 = B_2 = 0.5$ (same slip coefficient along the two plates). Since the leading eigenvalue decreases cessation becomes slower as slip is enhanced.

## 5.2 Slip with non-zero slip yield stress

When $V \leq V_c$, the standard no-slip solution applies. When $V > V_c$, the fluid initially slips along both walls.

As the velocity is reduced, slip ceases first along the lower plate and then along the upper one. Hence, there is no slip in the final stage of the cessation. The critical times for the cessation of slip along the lower and the upper walls are denoted by $t_{c1}$ and $t_{c2}$, respectively. For the rest of this section it is more convenient to scale the velocity by $V_c$, lengths by $H$, the stress by $\tau_c$, and time by $\eta/\tau_c$. Again, non-dimensionalized quantities are denoted by stars. Hence, the no-slip case corresponds to $V^* \leq 1$.

### 5.2.1 No-slip regime

The boundary and initial conditions read

$$\left.\begin{aligned}
u_x^*(0,t^*) = u_x^*(1,t^*) &= 0, & t^* &> 0 \\
u_x^*(y^*,0) &= y^*, & 0 &\leq y^* \leq 1
\end{aligned}\right\}$$
(75)

and the solution is given by

$$u_x^*(y^*,t^*) = \sum_{k=1}^{\infty} C_k^* \sin(\lambda_k y^*)e^{-\lambda_k^2 t^*},$$
(76)

where $\lambda_k = k\pi$, $k = 1, 2, \ldots$ and

$$C_k^* = -\frac{2V^*\cos\lambda_k}{\lambda_k}.$$
(77)

### 5.2.2 Slip along both walls ($V^* > 1$)

In this case the boundary and initial conditions read

$$\left.\begin{aligned}
u_x^*(0,t^*) &= B\left(\frac{\partial u_x^*}{\partial y^*}-1\right), & t^* &> 0 \\
u_x^*(1,t^*) &= -B\left(\frac{\partial u_x^*}{\partial y^*}+1\right), & t^* &> 0 \\
u_x^*(y^*,0) &= \frac{1}{1+2B}[(V^*+2B)y^*+B(V^*-1)], & 0 &\leq y^* \leq 1
\end{aligned}\right\}.$$
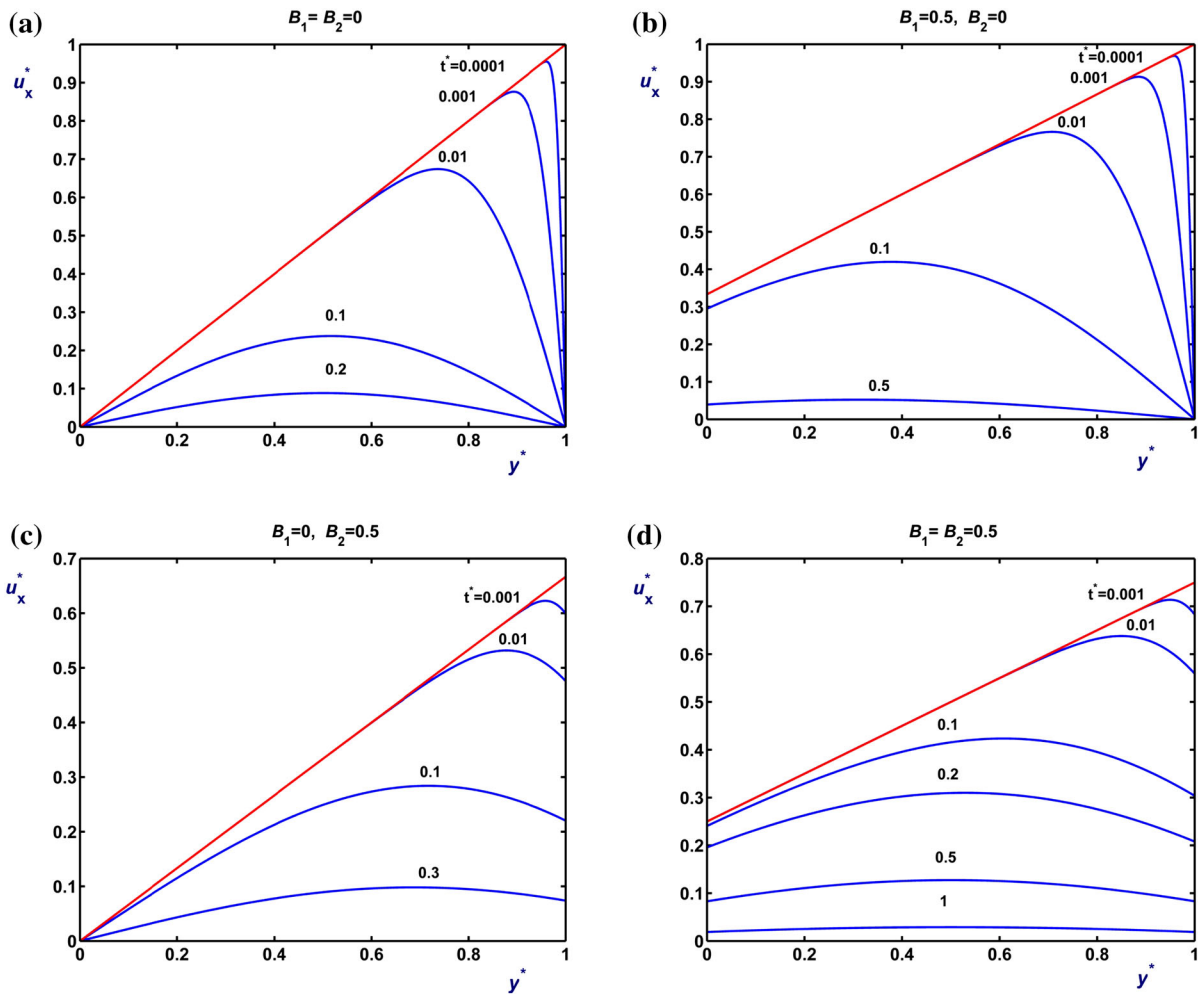(78)

The solution is given by

**Fig. 11** Cessation of simple shear flow: (a) No-slip along the walls ($B_1 = B_2 = 0$); (b) Navier slip only along the lower wall ($B_1 = 0.5$, $B_2 = 0$); (c) Navier slip only along the upper wall ($B_1 = 0$, $B_2 = 0.5$); (d) Navier slip along both walls ($B_1 = B_2 = 0.5$)

$u_x^*(y^*, t^*)$

$$
= \begin{cases} \sum\limits_{m=1}^{\infty} A_m^*[\sin(\mu_m y^*) + B\mu_m \cos(\mu_m y^*)]e^{-\mu_m^2 t^*} - B, & t^* \leq t_{c1}^* \\ \sum\limits_{n=1}^{\infty} C_n^* \sin(a_n y^*)e^{-a_n^2(t^*-t_{c1}^*)} - \dfrac{By^*}{B+1}, & t_{c1}^* < t^* \leq t_{c2}^* \\ \sum\limits_{k=1}^{\infty} D_k^* \sin(\lambda_k y^*)e^{-\lambda_k^2(t^*-t_{c2}^*)}, & t^* > t_{c2}^* \end{cases}
$$

(79)

where $\mu_m$ and $a_n$ are the roots of

$$\tan \mu_m = \frac{-2B\mu_m}{1 - B^2\mu_m^2} \tag{80}$$

and

$$\tan a_n = -Ba_n, \tag{81}$$

respectively. The constants $A_m^*$, $C_n^*$ and $D_k^*$ are given by

$$A_m^* = \frac{2\cos\mu_m(1 + \mu_m^2 B^2)(V^* + 2B)}{\mu_m(\mu_m^2 B^2 - 1)(\mu_m^2 B^2 + 2B + 1)}, \tag{82}$$

$$
C_n^* = \frac{-2B}{a_n(1 + B\cos^2 a_n)} \\
- \frac{2a_n B}{(1 + B\cos^2 a_n)}\sum_{m=1}^{\infty} \frac{\mu_m A_m^* e^{-\mu_m^2 t_{c1}^*}}{\mu_m^2 - a_n^2}
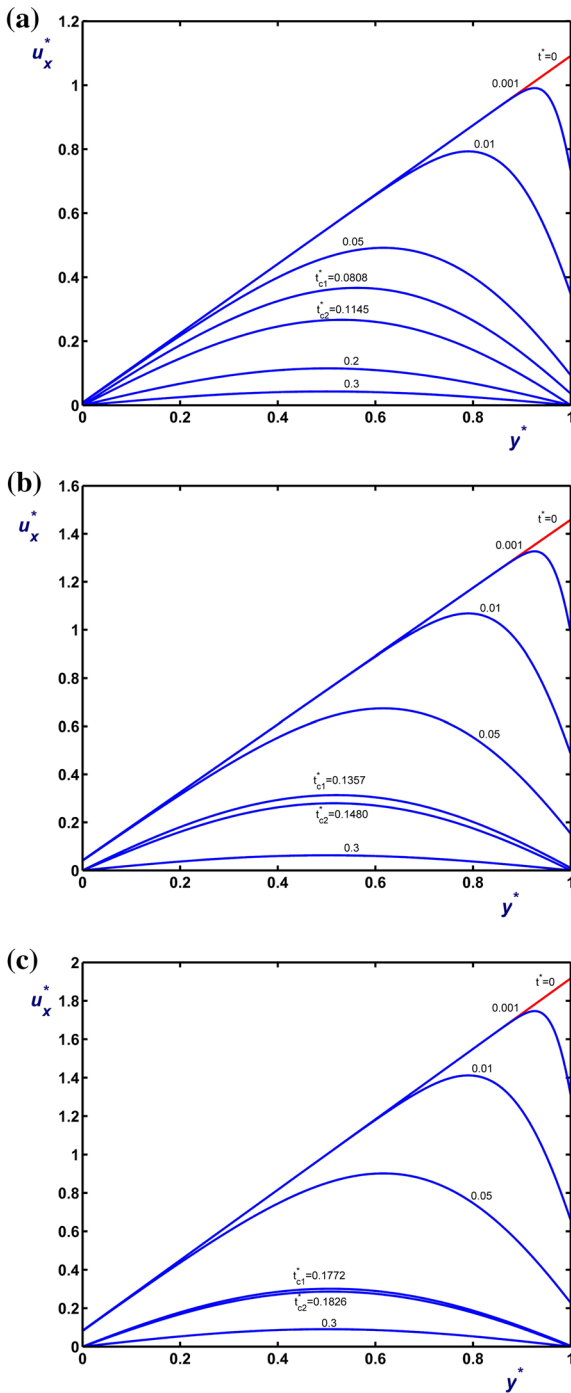\tag{83}
$$

and

**Fig. 12** Evolution of the velocity in cessation of simple shear flow with non-zero slip yield stress with $B = 0.1$: (a) $V^* = 1.1$; (b) $V^* = 1.5$; (c) $V^* = 2$
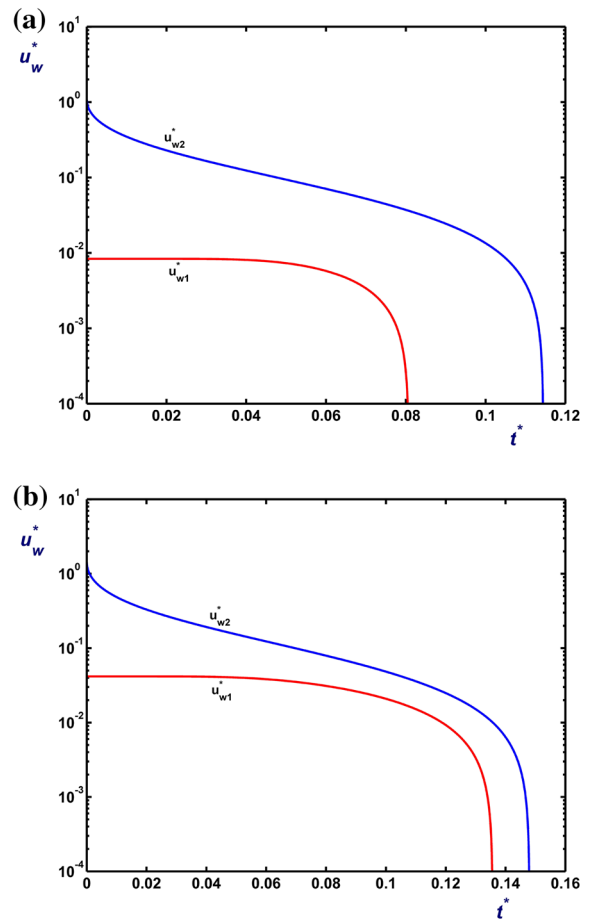


**Fig. 13** Evolution of the slip velocities in cessation of simple shear flow with non-zero slip yield stress with $B = 0.1$: (a) $V^* = 1.1$; (b) $V^* = 1.5$

$$D_k^* = \frac{2B\cos\lambda_k}{(B+1)\lambda_k} + 2\lambda_k\cos\lambda_k$$
$$\times \left\{\sum_{n=1}^{\infty} \frac{\sin a_n e^{-a_n^2(t_{c2}-t_{c1})}}{a_n^2 - \lambda_k^2}\left[\frac{-2B}{a_n(1+B\cos^2 a_n)} - \frac{2a_n B}{(1+B\cos^2 a_n)}\sum_{m=1}^{\infty} \frac{2\cos\mu_m\left(1+\mu_m^2 B^2\right)(V^*+2B)e^{-\mu_m^2 t_{c1}}}{\left(\mu_m^2 - a_n^2\right)\left(\mu_m^2 B^{2-1}\right)\left(\mu_m^2 B^2 + 2B + 1\right)}\right]\right\}.$$

$$(84)$$

The two slip velocities are given by

$$u_{w1}^*(t^*) = \begin{cases} \sum_{m=1}^{\infty} A_m^* B\mu_m e^{-\mu_m^2 t^*} - B, & t^* \le t_{c1}^* \\ 0 & t^* > t_{c1}^* \end{cases} \quad (85)$$

and

$$u_{w2}^*(t^*)$$
$$= \begin{cases} \sum_{m=1}^{\infty} A_m^*(\sin\mu_m + B\mu_m\cos\mu_m)e^{-\mu_m^2 t^*} - B, & t^* \le t_{c1}^* \\ \sum_{n=1}^{\infty} C_n^* \sin a_n e^{-a_n^2(t^*-t_{c1}^*)} - \frac{B}{B+1}, & t_{c1}^* < t^* \le t_{c2}^* \\ 0, & t^* > t_{c2}^* \end{cases}$$

$$(86)$$

The critical times $t_{c1}^*$ and $t_{c2}^*$ are the roots of

$$\sum_{m=1}^{\infty} A_m^* B\mu_m e^{-\mu_m^2 t_{c1}^*} - B = 0 \quad (87)$$

and

$$\sum_{n=1}^{\infty} C_n^* \sin a_n e^{-a_n^2(t_{c2}^*-t_{c1}^*)} - \frac{B}{B+1} = 0, \quad (88)$$

respectively. Keeping only the first terms of the above summations leads to the following estimates of the critical times:

$$\bar{t}_{c1}^* = \frac{1}{\mu_1^2}\ln\left(A_1^*\mu_1\right) \quad (89)$$

and

$$\bar{t}_{c2}^* = \bar{t}_{c1}^* + \frac{1}{a_1^2}\ln\frac{(B+1)C_1^* \sin a_1}{B}. \quad (90)$$

The evolution of the velocity for $B = 0.1$ and $V^* = 1.1, 1.5$ and 2 is illustrated in Fig. 12. The velocity profiles at $t_{c1}^*$ and $t_{c2}^*$ are provided in all cases. Figure 13 shows the evolution of the two slip velocities for $V^* = 1.1$ and 1.5. The lower-plate slip

velocity initially appears to be rather constant but eventually it decreases rapidly vanishing at $t_{c1}^*$. The upper-plate slip velocity, which is at least one order of magnitude greater, decays very fast initially and then fast to vanish at $t_{c2}^* > t_{c1}^*$. The effect of $V^*$ on the two slip velocities is also illustrated in Fig. 14. In general,
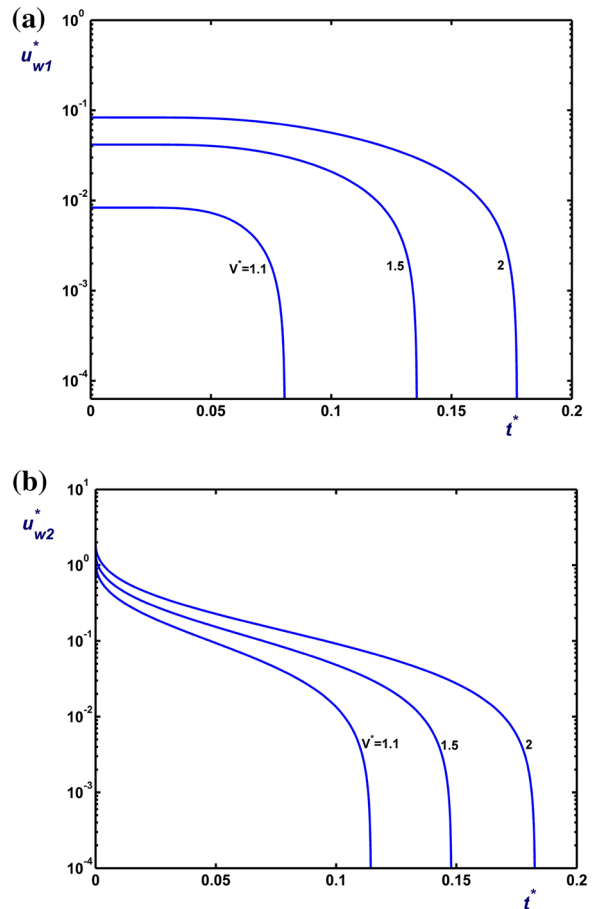
Fig. 14 Evolution of the slip velocities in cessation of simple shear flow with non-zero slip yield stress, for $B = 0.1$ and various values of $V^*$: (a) along the lower plate; (b) along the upper plate
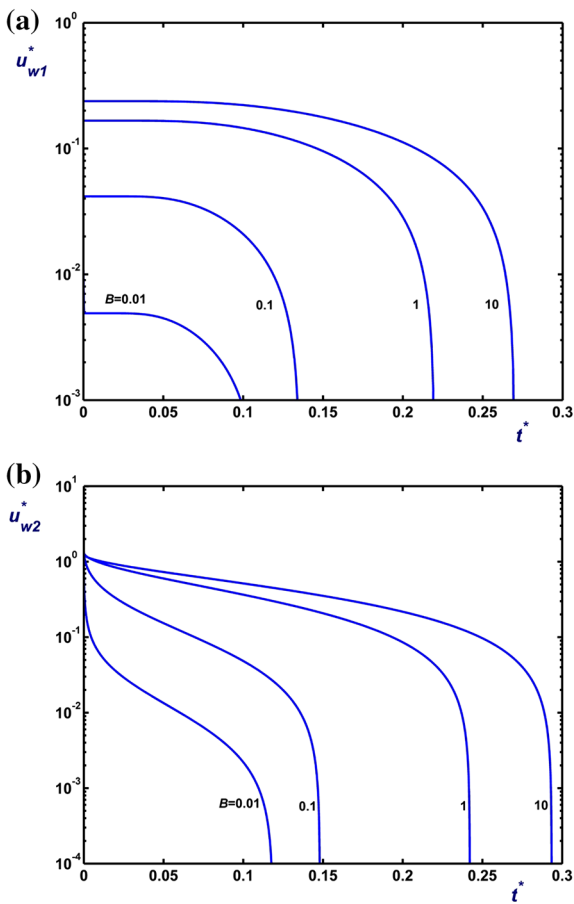
**Fig. 15** Evolution of the slip velocity in cessation of plane Couette flow with non-zero slip yield stress for $V^* = 1.5$ and various values of $B$: (a) lower plate; (b) upper plate
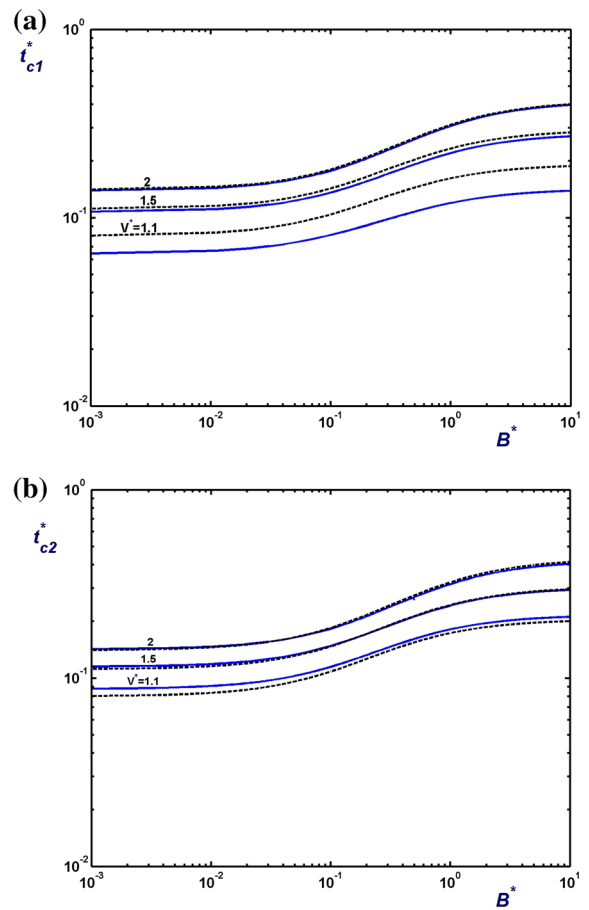


**Fig. 16** The critical times $t_{c1}^*$ and $t_{c2}^*$ for the cessation of plane Couette flow with non-zero slip yield stress for various values of $V^*$. The dashed lines are the estimates obtained using only the leading term of the corresponding series expansion, i.e. using Eqs. (89) and (90)

slip becomes stronger and cessation becomes slower and therefore the critical times $t_{c1}^*$ and $t_{c2}^*$ increase as $V^*$ is increased. Finally the effect of the slip number $B$ on the two slip velocities is illustrated in Figs. 15 and 16. In Fig. 15, one observes the evolution of the two slip velocities for $V^* = 1.5$ and different values of $B$. The decay of the slip velocities is slower as the slip number $B$ is increased, i.e. when slip is stronger. Figure 16 shows plots of the critical times $t_{c1}^*$ and $t_{c2}^*$ for the cessation of slip along the lower and upper plates, respectively, versus the slip number $B$ for various values of $V^*$. As already discussed the values of the two critical times increase with $B$. In Fig. 8, the estimates of the stopping times given by Eqs. (89) and (90) are also compared with the exact values. It is shown that the value of $t_{c1}^*$ is overestimated while that

of $t_{c2}^*$ is underestimated. The estimates are improved as the values of $B$ and $V^*$ are increased.

## 6 Conclusions

We have solved both the steady-state and time-dependent circular and plane Couette flows of a Newtonian fluid with wall slip following the two-branch slip equation proposed by Spikes and Granick [18]. The latter involves a non-zero slip yield stress above which the variation of the wall shear stress with the slip velocity is linear. The solutions presented here supplement the analytical solutions reported by Ng [14] and Kaoullas and Georgiou [11, 12] and may be

useful in correcting slip effects in Couette rheometry, in checking numerical non-Newtonian simulation codes, and in start up and cessation of steady shear in MEMS devices.

The existence of non-zero slip yield stress results in three steady-state regimes for the circular Couette flow. These are defined by the two critical values of the angular velocity at which slip is triggered along the rotating inner cylinder and the fixed outer one. In cessation of the flow in the last regime where slip is present along both cylinders, it has been shown that slip ceases first finite along the outer cylinder and then along the inner one.

In the case of steady plane Couette flow, there are two flow regimes, since slip occurs only above a critical value of the velocity of the moving upper plate, $V_c$. Given that the shear stress in the flow domain is constant, the slip velocities $u_{w1}$ and $u_{w2}$ along the lower and upper plates are equal. In time-dependent flow slip may occur only along one of the two plates. In the case of flow cessation above $V_c$, there are three flow regimes defined by two critical times $t_{c1}$ and $t_{c2}$, respectively defined as the times at which slip ceases along the lower and the upper plates. For times after $t_{c2}$, the flow decays exponentially with no slip.

**Compliance with ethical standards**

**Conflict of interest**  The authors declare that they have no conflict of interest.

# References

1. Rothstein JP (2010) Slip on superhydrophoboc surfaces. Ann Rev Fluid Mech 42:89–109
2. Hatzikiriakos SG (2012) Wall slip of molten polymers. Prog Polym Sci 37:624–643
3. Neto C, Evans DR, Bonaccurso E, Butt HJ, Craig VSJ (2005) Boundary slip in Newtonian liquids: a review of experimental studies. Rep Prog Phys 68:2859–2897
4. Lauga E, Brenner MP, Stone HA (2007) Microfluidics: the no-slip boundary condition, Chapter 19. In: Tropea C, Yarin AL, Foss JF (eds) Handbook of experimental fluid dynamics. Springer, Heidelberg
5. Bonaccurso E, Kappl M, Butt HJ (2002) Hydrodynamic force measurement: boundary slip of water on hydrophilic surfaces and electrokinetic effects. Phys Rev Lett 88:076103-1–076103-4
6. Jabbarzadeh A, Atkinson JD, Tanner RI (1999) Wall slip in the molecular dynamics simulation of thin films of hexadecane. J Chem Phys 111:2612–2620
7. Navier CLMH (1827) Sur les lois du mouvement des fluides. Mem Acad R Sci Inst Fr 6:389–440
8. Denn MM (2001) Extrusion instabilities and wall slip. Ann Rev Fluid Mech 33:265–287
9. De Gennes PG (2002) On fluid/wall slippage. Langmuir 18:3413–3414
10. Chatzimina M, Georgiou G, Alexandrou AN (2009) Circular Couette flows of viscoplastic fluids. Appl Rheol 19:34288
11. Kaoullas G, Georgiou GC (2013) Newtonian Poiseuille flows with wall slip and non-zero slip yield stress. J Non Newton Fluid Mech 197:24–30
12. Kaoullas G, Georgiou GC (2013) Slip yield stress effects in start-up Newtonian Poiseuille flows. Rheol Acta 52:913–925
13. Ferrás LL, Nóbrega JM, Pinho FT (2012) Analytical solutions for Newtonian and inelastic non-Newtonian flows with wall slip. J Non Newton Fluid Mech 175:76–88
14. Ng C (2016) Starting flow in channels with boundary slip. Meccanica. doi:10.1007/s11012-016-0384-4
15. Sochi T (2011) Slip at fluid-solid interface. Polym Rev 51:309–340
16. Damianou Y, Georgiou GC, Moulitsas I (2013) Combined effects of compressibility and slip in flows of a Herschel–Bulkley fluid. J Non Newton Fluid Mech 193:89–102
17. Damianou Y, Philippou M, Kaoullas G, Georgiou GC (2014) Cessation of viscoplastic Poiseuille flow with wall slip. J Non Newton Fluid Mech 203:24–37
18. Spikes H, Granick S (2003) Equation for slip of simple liquids at smooth solid surfaces. Langmuir 19:5065–5071
19. Djoko J, Koko J (2016) Numerical methods for the Stokes and Navier–Stokes equations driven by threshold slip boundary conditions. Comput Methods Appl Mech Eng 305:936–958
20. Damianou Y, Georgiou GC (2014) Viscoplastic Poiseuille flow in a rectangular duct with wall slip. J Non Newton Fluid Mech 214:88–105
21. Georgiou GC, Kaoullas G (2013) Newtonian flow in a triangular duct with slip at the wall. Meccanica 48:2577–2583
22. Tauviqirrahman M, Jamari M, Schipper DJ (2014) Numerical study of the load-carrying capacity of lubricated parallel sliding textured surfaces including wall slip. Tribol Trans 57:134–145
23. Bryan MP, Rough SL, Wilson DI (2015) Investigation of static zones and wall slip through sequential ram extrusion of contrasting micro-crystalline cellulose-based pastes. J Non Newton Fluid Mech 220:57–68
24. Macosko CW (1994) Rheology: principles, measurements and applications. VCH Publishers, New York
25. Papanastasiou TC, Georgiou GC, Alexandrou AN (2000) Viscous fluid flow. CRC Press, Boca Raton